HHS Public Access

Author manuscript

Circ Cardiovasc Imaging. Author manuscript; available in PMC 2021 October 20.

Published in final edited form as:

Circ Cardiovasc Imaging. 2020 October ; 13(10): e010586. doi:10.1161/CIRCIMAGING.120.010586.

Imaging cardiovascular and lung macrophages with the PET sensor ^{64}Cu-Macrin in mice, rabbits and pigs

Matthias Nahrendorf, MD PhD[1,2,3,4,16,*], **Friedrich Felix Hoyer, MD**[1,2,16], **Anu E. Meerwaldt, MSc**[5,6], **Mandy M.T. van Leent, PhD**[5,7], **Max L. Senders, MD**[5,7], **Claudia Calcagno, PhD**[5], **Philip M. Robson, PhD**[5], **George Soultanidis, PhD**[5], **Carlos Pérez-Medina, PhD**[5,8], **Abraham J.P. Teunissen, PhD**[5], **Yohana C. Toner, BSc**[5], **Kiyotake Ishikawa, MD**[9], **Kenneth Fish, PhD**[9], **Ken Sakurai, PhD**[5], **Esther M. van Leeuwen, MSc**[5,6], **Emma D. Klein, MSc**[5], **Alexandros Marios Sofias, PhD**[5,10], **Thomas Reiner, PhD**[11], **David Rohde, MD**[1,2], **Aaron D. Aguirre, MD**[1,3,12], **Gregory Wojtkiewicz, MSc**[1], **Stephen Schmidt, BSc**[1], **Yoshiko Iwamoto, BSc**[1], **David Izquierdo-Garcia, PhD**[13], **Peter Caravan, PhD**[13], **Filip K. Swirski, PhD**[1,2], **Ralph Weissleder, MD PhD**[1,2,13,14], **Willem J.M. Mulder, PhD**[5,7,15]

[1]Center for Systems Biology, Massachusetts General Hospital and Harvard Medical School, Boston, MA, USA. [2]Department of Radiology, Massachusetts General Hospital and Harvard Medical School, Boston, MA, USA. [3]Cardiovascular Research Center, Massachusetts General Hospital and Harvard Medical School, Boston, MA, USA. [4]Department of Internal Medicine I, University Hospital Wuerzburg, Wuerzburg, Germany. [5]Biomedical Engineering and Imaging Institute, Icahn School of Medicine at Mount Sinai, New York, NY, USA. [6]Biomedical MR Imaging and Spectroscopy Group, Center for Image Sciences, University Medical Center Utrecht and Utrecht University, Utrecht, The Netherlands. [7]Department of Medical Biochemistry, Amsterdam University Medical Centers, University of Amsterdam, Amsterdam, The Netherlands. [8]Centro Nacional de Investigaciones Cardiovasculares, Madrid, Spain. [9]Cardiovascular Research Center, Department of Cardiology, Icahn School of Medicine at Mount Sinai, New York, NY, USA. [10]Department of Circulation and Medical Imaging, Faculty of Medicine and Health Sciences, Norwegian University of Science and Technology, Trondheim, Norway. [11]Department of Radiology and Chemical Biology Program, Memorial Sloan-Kettering Cancer Center; Department of Radiology, Weill Cornell Medical College, New York, NY, USA. [12]Wellman Center for Photomedicine, Massachusetts General Hospital and Harvard Medical School, Boston, MA, USA. [13]The Institute for Innovation in Imaging, A. A. Martinos Center for Biomedical Imaging, Massachusetts General Hospital and Harvard Medical School, Charlestown, MA, USA. [14]Department of Systems Biology, Harvard Medical School, Boston, MA, USA. [15]Department of Oncological Sciences, Icahn School of Medicine at Mount Sinai, New York, NY, USA; Laboratory of Chemical Biology, Department of Biomedical Engineering and Institute for Complex Molecular

[*]Corresponding authors: rweissleder@hms.harvard.edu, mnahrendorf@mgh.harvard.edu. Phone: 617-643-0500, Address: Center for Systems Biology, Massachusetts General Hospital, Richard B. Simches Research Center, 185 Cambridge Street, Suite 5.210, Boston, MA 02114, USA.

Disclosures

M.N. has received funds or material research support from Novartis, GSK, Pfizer, GlycoMimetics, Medtronic, Biotronik, Alnylam and CSL Behring and consulting fees from Verseau Therapeutics, Sigilon, Molecular Imaging Inc., IFM Therapeutics, Gimv and Biogen.

Systems, Eindhoven University of Technology, Eindhoven, The Netherlands. [16]These authors contributed equally: Matthias Nahrendorf, Friedrich Felix Hoyer.

Abstract

Background——Macrophages, innate immune cells that reside in all organs, defend the host against infection and injury. In the heart and vasculature, inflammatory macrophages also enhance tissue damage and propel cardiovascular diseases.

Methods——We here use in vivo positron emission tomography (PET) imaging, flow cytometry and confocal microscopy to evaluate quantitative noninvasive assessment of cardiac, arterial and pulmonary macrophages using the nanotracer ^{64}Cu-Macrin, a 20 nm spherical dextran nanoparticle assembled from non-toxic polyglucose.

Results——PET imaging using ^{64}Cu-Macrin faithfully reported accumulation of macrophages in the heart and lung of mice with myocardial infarction, sepsis or pneumonia. Flow cytometry and confocal microscopy detected the near-infrared fluorescent version of the nanoparticle (^{VT680}Macrin) primarily in tissue macrophages. In 5-day-old mice, ^{64}Cu-Macrin PET imaging quantified physiologically more numerous cardiac macrophages. Upon intravenous administration of ^{64}Cu-Macrin in rabbits and pigs, we detected heightened macrophage numbers in the infarcted myocardium, inflamed lung regions and atherosclerotic plaques using a clinical PET/magnetic resonance imaging (MRI) scanner. Toxicity studies in rats and human dosimetry estimates suggest that ^{64}Cu-Macrin is safe for use in humans.

Conclusions——Taken together, these results indicate ^{64}Cu-Macrin could serve as a facile PET nanotracer to survey spatiotemporal macrophage dynamics during various physiological and pathological conditions. ^{64}Cu-Macrin PET imaging could stage inflammatory cardiovascular disease activity, assist disease management and serve as an imaging biomarker for emerging macrophage-targeted therapeutics.

Clinical summary—Ushered in by high-dimensional diagnostic tools such as flow cytometry and single cell RNA-sequencing, the knowledge on the immune system's role in homeostasis and disease is rapidly expanding. The last decade has seen a considerable expansion of known immune cell subsets and their functions. Cardiovascular organs and cardiovascular disease are no exemption: for instance, we now understand that not only atherosclerotic plaques or ischemic, inflamed myocardium contains leukocytes, but that these cells are present in the steady-state heart and participate in organ development, homeostatic functions such as metabolism and conduction, tissue regeneration, matrix remodeling and recovery from disease. The field is on the verge of translating this insight into new cures; however, clinical tools to monitor the immune system, and more specifically immune cells, are still mostly limited to counting them in blood samples. This is a severe limitation as circulating immune cells do not necessarily correlate with the numbers and phenotypes of cells residing in tissues. Organ biopsies are likewise limited given their invasiveness and inherent sampling errors. We here provide insight into PET imaging agent development targeting macrophages. Based on small biodegradable nanoparticles derivatized with either a PET isotope of a fluorochrome, we characterize the utility of Macrin nanoparticles in several physiological and pathological settings. Since macrophages are emerging as high-value therapeutic

targets, we anticipate that the described quantitative imaging tools will catalyze drug development and clinical trials.

Keywords

imaging; nanoparticle; macrophages; heart; myocardial infarction; pneumonia; atherosclerosis

Subject codes

Inflammation; Imaging; Atherosclerosis; Myocardial infarction

Introduction

Tissue macrophages pursue heterogeneous functions[1, 2] and populate organs with varying density in health and disease[3]. In the steady-state heart, arterial wall, lung and brain, among other organs, these cells suppress inflammation and contribute to tissue homeostasis. After sterile or infectious injuries, macrophages initiate and amplify immune responses to limit tissue damage and intercept bacterial intruders. While many macrophage functions protect the host, exuberant inflammatory actions and macrophage oversupply may compromise cardiovascular health[3].

Expanding macrophage populations are a characteristic system-wide feature in inflammatory cardiovascular conditions. At primary injury and remote disease sites[4], additional cells either derive from monocytes, i.e. they are recruited from hematopoietic organs, or they arise through local proliferation from macrophages that resided in the previously healthy tissue. Both processes co-exist in atherosclerotic plaque and in diseased myocardium, increasing macrophage numbers by orders of magnitude[3]. If macrophages become too abundant, they propagate inflammatory tissue destruction, cardiovascular disease progression and poor clinical outcomes. For instance, macrophage oversupply in acute myocardial infarction and in the remote myocardium leads to heart failure in mice[5], which is paralleled by the clinical association between systemic monocyte numbers and cardiovascular events[6–8]. Macrophages of varying phenotypes are also involved in heart regeneration; emerging data indicate that these cells support enhanced healing after myocardial infarction in newborn mice[9]. Finally, macrophages also sense remote injury and determine host resilience against infection. These functions may either propagate inflammatory complications and multi-organ failure or support elimination of bacteria[4].

For these reasons, macrophages and their inflammatory products are being investigated as highly promising therapeutic targets. One obstacle in this discovery process is the lack of noninvasive assays to quantify tissue macrophages. Since macrophages rely on not only recruitment from the blood stream but also local proliferation in the tissue, circulating monocyte numbers are not always a suitable surrogate for tissue macrophage content. Biopsies are more reliable but only report on small specimen rather than entire organ systems, giving rise to sampling error. Biopsy of the myocardium and atherosclerotic plaques is not commonly pursued due to the threat of complications. Therefore, there is an

unmet need for a noninvasive imaging assays that quantify tissue macrophages across the body.

Molecularly targeted imaging agents contribute to our insight into molecular and cellular mechanisms of inflammatory diseases, including coronary heart disease. Although numerous molecular imaging agents targeting inflammatory cells have been developed and validated in small animals[10], only a few are currently in clinical use. For example, ^{18}FDG[11] and ^{68}Ga-pentixafor[12] were used in patients with acute myocardial infarction, reporting on glucose uptake and the presence of the chemokine receptor CXCR4, respectively. These two targets are tightly related to inflammation; however, they are not specific for macrophages. Some promising macrophage imaging agents, for instance targeting these cells' surface receptors[13, 14], are advancing through development; however, given the heterogeneity of macrophages, such strategies may not report on certain cell subsets that do not express the targets.

To assay macrophages non-invasively, we developed a macrophage sensor called Macrin. This 20 nm spherical nanoparticle evolved through several iterations of adjusting physico- and radio-chemical properties to optimize pharmacokinetics and targeting of macrophages. Here we explored the utility of the latest-generation material[15] to quantify macrophages in physiological settings as well as cardiovascular and pulmonary inflammation. We examined the feasibility of ^{64}Cu-Macrin PET macrophage imaging in a basket trial of small and large animals with clinically relevant heart disease but also in the heart of newborn mice and in pneumonia (Fig. 1A, Online Table I) to test the assay in physiological settings and pathologies with various causes and degrees of inflammation. These experiments revealed the sensitivity and versatility of Macrin PET across inflammatory conditions. We further report that rodent toxicity studies and human radiation dose estimates suggest that Macrin is safe for first-in-human studies.

Methods

We confirm that the manuscript adheres to the Transparency and Openness Promotion (TOP) guidelines. The data that support the findings of this study are available from the corresponding author upon reasonable request. All experiments were approved by the Institutional Animal Care and Use Committee (IACUC) of the Massachusetts General Hospital or Icahn School of Medicine at Mount Sinai. Online Table I summarizes all experiments performed (including goals, model, interventions and animal numbers). An Online Materials and Methods section contains additional information on procedures.

Mouse PET/CT

PET/CT (Inveon, Siemens, Munich, Germany) imaging was done 24 hours post injection of ^{64}Cu-Macrin (~230 μCi in 150 μL saline for adult mice via tail-vein injection and ~50 μCi in 30 μL saline for 5-day-old mice via retro-orbital injection). Primary end point was increased standard uptake value (SUV) in inflamed tissue, the only exclusion criterion was death prior imaging. High-resolution CT was acquired prior to serial 30-minute static PET with the following parameters: beam energy of 80 kVp, current 500 μA X-ray and exposure time of 425 ms over 360 projections. PET images were reconstructed using a 3D ordered-subset

expectation maximization/maximum a posteriori (3D-OSEM/MAP). Voxel count rates in the reconstructed images were decay corrected and converted to SUV by system calibration factor from a cylindrical phantom. Regions of interest (ROI) analyses were guided by co-registered anatomic CT images to yield organ activity normalized by the body weight (g) and the residual activity at scan.

Mouse PET/MR

Mice were injected intravenously with ^{64}Cu-Macrin (218.3±41.1 μCi) via tail vein. PET/CT and MRI were conducted sequentially as described previously[16]. Under isoflurane anesthesia (2% in oxygen), mice were positioned on a custom-designed mouse bed compatible with both PET/CT and MRI. Mice were imaged with CT followed by static PET scans (30 minutes) ~24 hours after tracer administration on an Inveon small animal PET/CT scanner (Siemens, Munich, Germany). MRI was performed on a 4.7 Tesla Bruker PharmaScan MRI scanner (Billerica, MA) with a cardiac coil in birdcage design (RAPID MR international, Columbus, OH). A fast low angle shot (FLASH) sequence was used with integrate cardiac and respiratory gating with the following parameters: TE=2.94, TR=10 ms, FA=18°, matrix size=200 × 200 × 1, voxel size=0.15 × 0.15 × 1 mm^3. Delayed enhancement was imaged 10 minutes post intravenous injection of gadolinium-diethylenetriamine pentaacetic acid (Gd-DTPA, 30 μL).

PET/MR rabbits

All rabbits were imaged with a clinical PET/MR system (Siemens 3T Biograph mMR). The rabbits received an intravenous injection of ^{64}Cu-Macrin (59.57–00.3 MBq) via marginal ear vein one day before imaging. Anesthesia was induced by intramuscular injection of ketamine (20 mg/kg) (Fort Dodge Animal Health) and xylazine (0.5 mg/kg) (Bayer). Rabbits were placed in a 6-channel body matrix coil, received isoflurane anesthesia at 1.5% by inhalation and were oxygenated for the remainder of the PET/MR imaging experiment while vital parameters were monitored. PET was acquired for thorax and abdomen, 60 minutes and 20 minutes, respectively, in caudocranial direction. During PET of the thorax, cardiac cine MR images were acquired for cardiac function measurement using retrospective gating and free breathing. Images were acquired using a fast low angle shot (FLASH) sequence, with the following imaging parameters: repetition time (TR) 64.64 ms, echo time (TE) 3.76 ms, flip angle 12°, number of averages 12, 14–15 interleaved slices with no gap, 15 cardiac frames, 3 mm slice thickness, reconstructed spatial resolution 0.729×0.729 mm^2. In parallel with abdominal PET, MR time-of-flight (TOF) non-contrast enhanced angiography images were acquired to delineate the abdominal aorta, with the following imaging parameters: TR 25 ms, TE 2.8 ms, flip angle 20°, number of averages 1, 200 slices, slice thickness 1 mm, reconstructed spatial resolution 0.35×0.35 mm^2. PET reconstruction was performed using Siemens E7 tools. Attenuation correction of PET images was performed using a vendor built-in Dixon MR-based attenuation map (MR-AC) with 2 (soft tissue, air). Images were reconstructed using a 3D ordinary Poisson ordered subsets expectation maximization (OP-OSEM) algorithm with point-spread-function (PSF) resolution modeling, using 3 iterations and 21 subsets and filtered with a 4 mm Gaussian filter.

PET/MR pigs

Six Yucatan miniature pigs underwent imaging with a clinical PET/MR system (Siemens 3T Biograph mMR) before and after myocardial infarction. In addition, two Yorkshire pigs were included as controls and imaged once. All pigs received an intravenous injection of ^{64}Cu-Macrin (85.9 – 268.6 MBq) via marginal ear vein one day before each imaging session. Anesthesia was induced by intramuscular injection of tiletamine and zolazepam (6 – 10 mg/kg, Telazol, Zoetis). Pigs were intubated and placed on the scanner bed and were anesthetized with isoflurane at 1.5–2% supplemented with oxygen for the remainder of the PET/MR imaging experiment. Vital parameters were monitored. Six-channel body matrix coils were placed on the thorax and used for signal reception. Following scout scans, a multi-bed step-and-shoot PET was acquired within 20 mins (pelvis; abdomen) or 60 mins (thorax).

During thoracic PET/MR acquisition, cardiac cine and late gadolinium enhancement MR images were acquired for cardiac function and infarct detection, respectively. Cine short stack images were acquired using a True FISP sequence with retrospective ECG gating. Imaging parameters were: TR 46.62 ms, TE 1.51 ms, flip angle 45°, number of averages 1, 16–22 interleaved slices with no gap, 25 cardiac frames, 4mm slice thickness, reconstructed spatial resolution 1.875×1.875 mm^2. Late gadolinium (0.1 mmol/kg, Magnevist, Bayer) enhancement images were acquired using a FLASH sequence with prospective ECG triggering as follows: TR equivalent to 1 R-R period (mean 530.7, SD 112.4 ms), TE 2.21 ms, flip angle 20°, number of averages 1, 20 slices, slice thickness 4 mm, reconstructed spatial resolution 1.367×1.367mm^2. In both cases, acquisition was performed with assisted breath holds enacted by briefly closing the ventilator.

In pigs, attenuation correction of PET images was performed using 4 tissue compartments (soft tissue, fat, lung and air) and images reconstructed as described for rabbits.

PET/MR data analysis rabbit and pigs

All data were processed using Osirix MD v 9.5.1 (OsiriX Foundation, Geneva, Switzerland). Multiple regions of interest (ROIs) (≥ 6 per organ) were manually drawn. Anatomical images were overlaid with reconstructed PET images and SUVs of ROIs were exported with the ‘Export ROIs’ plugin. Cardiac function was analyzed by manually segmenting end systolic and diastolic volumes and quantifying ejection fraction with the MRHeart plugin[17].

Statistics

Results are expressed as mean ± standard error or standard deviation. GraphPad Prism 8.0c for Macintosh (GraphPad Software Inc.) was used for statistical analysis. The number of animals used is indicated as dot overlay in all bar graphs unless indicated otherwise in the figure legends. Differences between groups were evaluated by two-tailed t-tests or ANOVA tests for two-group and multi-group comparisons, respectively. Animals were randomely assigned to groups where possible (i.e. MI versus no MI). Blinding was not possible as disease group assignment was obvious from images and clinical status. Power estimation and group size was based on prior imaging studies with the nanoparticle[15]. A p value of <0.05 was used to indicate statistical significance.

Results

Pharmacokinetic profile and biodistribution of ^{64}Cu-Macrin in mice, rabbits and pigs

We first recorded the in vivo biodistribution of ^{64}Cu-Macrin (Fig. 1B) in healthy C57BL/6J mice at 4 and 24 hours after intravenous administration. Representative PET images (Online Fig. IA) and signal quantification as SUV (Online Fig. IB) demonstrated ^{64}Cu-Macrin uptake in macrophage-rich organs of the mononuclear phagocyte system, i.e. liver and spleen, which was confirmed by ex vivo scintillation counting at 1, 4, 24 and 48 hours after ^{64}Cu-Macrin injection (Online Table II). Of note, low accumulation was detected in the brain (0.27 % injected dose/g) and bone (2.78 % injected dose/g) at 24 hours post injection. 50.5% of the injected ^{64}Cu-Macrin dose was detected in the kidneys, possibly due to renal excretion of the small-sized particles. The remaining whole-body radioactivity was 12.01% of the injected dose 24 hours post injection. The blood activity and the heart-to-blood signal ratio (Online Fig. II) indicated that 24 hours after injection is a suitable imaging time point. ^{64}Cu-Macrin pharmacokinetics in rabbits showed a blood half-life of 45.1±24.6 minutes based on a two-phase exponential decay model (Online Fig. IIIA). In rabbits and pigs, we likewise observed high ^{64}Cu-Macrin uptake in macrophage-rich organs such as liver and spleen (Online Fig. IIIB–C).

In vivo quantitation of cardiac macrophages in mice, rabbits and pigs with acute myocardial infarction

Acute MI elicits a strong systemic inflammatory response that increases the number of macrophages robustly. Cardiac macrophages, in particular the inflammatory response after MI, are emerging therapeutic targets[2], which is why we examined whether cardiac macrophage fluctuations could be quantitatively assessed using ^{64}Cu-Macrin. ^{64}Cu-Macrin was intravenously administered to mice on day 4 after MI, and PET/CT and MRI was performed 24 hours post injection. ^{64}Cu-Macrin accumulated in the infarcted myocardium (Fig. 1C), which showed a 1.6-fold higher SUVs in comparison to control mice without MI (Fig. 1D). Ex vivo scintillation counting confirmed these data (Fig. 1E). Short axis rings of heart tissue were then processed for triphenyltetrazolium chloride (TTC) staining and autoradiography, confirming ^{64}Cu-Macrin accumulation in the infarcted area ex vivo (Fig. 1F). To assess whether the infarct signal derives from the intra- or extracellular space, we performed ex vivo scintillation counting of infarct tissue followed by scintillation counting of cells isolated from the infarct on day 4 after MI. Macrin activity was 3.3-fold higher in the cell pellet compared to infarct tissue (Online Fig. IV).

We next examined the cellular distribution of ^{VT680}Macrin, a fluorescent analog of ^{64}Cu-Macrin, with flow cytometry (Fig. 1G–J, Online Fig. V). In the heart, ^{VT680}Macrin was predominantly taken up by macrophages (Fig. 1H), in particular by MHCII^{high} and CCR2^{high} macrophage subsets (Online Fig. VA–C). Fibroblasts, endothelial cells and other immune cells such as CD11C^{high} leukocytes and Ly6G^{high} neutrophils, showed negligible uptake (Online Fig. VD–F). The mean fluorescent intensity (MFI) per macrophage, i.e. their individual ^{VT680}Macrin uptake, declined in the MI (Fig. 1I) while the number of Macrin^{+} macrophages expanded (Fig. 1J). The correlation between Macrin accumulation in the heart

and macrophage tissue density demonstrated that Macrin uptake was determined by cell density (Online Fig. VI).

To supplement quantitative FACS with anatomical distribution data, we investigated ^{VT680}Macrin cellular localization using confocal microscopy in Cx3cr1$^{GFP/+}$ mice, in which macrophages express high levels of green fluorescent protein (GFP)[18]. As expected, GFP^{+} macrophages expanded in infarcted myocardium (Fig. 1K–L). Confocal images demonstrated nanoparticle co-localization with GFP^{+} heart macrophages (Fig. 1M). Immunostaining of infarcted mouse hearts confirmed co-localization of Macrin with macrophages but not myocytes, endothelial cells or fibroblasts (Online Fig. VIIA–D).

Given the encouraging observations in mice with MI, we next used a clinical PET/magnetic resonance imaging (MRI) scanner to pursue imaging in large animals, a typical next step to evaluate whether a molecular imaging approach has clinical potential. Similar to mice, we observed a focal increase of PET signal in the infarcted myocardium (Fig. 2A) while MRI reported a decreased ejection fraction (Fig. 2B). The 27% increased SUVmax measured by PET (Fig. 2C) was confirmed by both ex vivo scintillation counting (Fig. 2D) and autoradiography exposure of rabbit heart slices (Fig. 2E). We obtained comparable results in pigs 3 days after ischemia reperfusion (Fig. 2F–J), which decreased the ejection fraction (Fig. 2G). Pig hearts were large enough to quantify ^{64}Cu-Macrin uptake in the 17 myocardial segments of the AHA circumferential polar plot used in clinical nuclear cardiology[19]. The 50% increased PET signal in infarcted segments (Fig. 2H) was corroborated by ex vivo tissue activity counting (Fig. 2I). Autoradiography exposure of excised pig hearts showed highest activity in the infarcted area (Fig. 2J). Hematoxylin and eosin (H&E) and immunohistochemistry staining for macrophages confirmed increased leukocyte and macrophage numbers in rabbit and pig infarcts (Online Fig. VIIE–J).

^{64}Cu-Macrin PET detects physiological differences in cardiac macrophage content

Recent studies linked better recovery from myocardial injury to increased cardiac macrophages in very young mice[9, 20, 21], which motivated us to investigate cardiac macrophages from newborn mice using ^{64}Cu-Macrin PET imaging. Five-day-old mice weighed only 3.2±0.1g and had a heart weight of 18.6±0.7mg, which is 7- and 6-fold lighter than 10-week-old adult mice (Fig. 3A–B), respectively (Fig. 3C). Despite this, ^{64}Cu-Macrin PET imaging (Fig. 3D) detected 1.7-fold higher cardiac signal in newborn mice, which was corroborated by ex vivo scintillation counting (Fig. 3E–F). Flow cytometric analysis of young and adult mouse hearts confirmed predominant ^{VT680}Macrin accumulation in cardiac macrophages (Fig. 3G–H). Interestingly, cardiac macrophages' phagocytic activity was higher in newborn mice (Fig. 3I), in which more cells had taken up the nanoparticle (Fig. 3J). Flow cytometry (Fig. 3K) and confocal microcopy of Cx3cr1$^{GFP/+}$ mice (Fig. 3L–M) confirmed higher macrophage numbers in the myocardium of 5-day-old mice when compared to 10-week-old adult mice (~22% difference by flow cytometry). Confocal images of GFP^{+} macrophages documented ^{VT680}Macrin uptake in young hearts (Fig. 3N).

^{64}Cu-Macrin PET senses systemic macrophage adaptions after remote injury

We next explored if ^{64}Cu-Macrin PET detects subtle systemic adaptions of the innate immune system that are remote from the site of injury or a septic focus, because our recent studies[4] indicate that tissue macrophages may play a role in remote organ resilience and complications. Sepsis can cause heart failure, and patients with myocardial infarction may develop edema and pneumonia. We thus tested whether ^{64}Cu-Macrin PET imaging can monitor heart macrophages in mice with peritonitis or lung macrophages after acute MI.

^{64}Cu-Macrin PET reported a 32% myocardial signal increase on day 5 after sepsis induction (Fig. 4A–B), which was corroborated by ex vivo scintillation counting of the heart (Fig. 4C). Flow cytometric analysis (Fig. 4D) revealed that ^{VT680}Macrin uptake decreased in individual cardiac macrophages after CLP (Fig. 4E–F); however, the total number of macrophages that incorporated the fluorescent nanoparticle increased (Fig. 4G). A sepsis-induced surge in cardiac macrophages was confirmed by confocal microscopy (Fig. 4H–I).

Recently, we discovered that acute MI primes lung macrophages via interferon-ɣ, which influenced bacterial clearance from mouse lungs[4]. We therefore employed ^{64}Cu-Macrin PET to study macrophages in the lungs of mice 5 days after MI. We observed patchy ^{64}Cu-Macrin uptake in the lung (Fig. 5A) and an 1.7-fold higher lung SUVmax after MI (Fig. 5B). Compared to mice without MI, ^{64}Cu-Macrin lung activity increased 2.4-fold by ex vivo scintillation counting (Fig. 5C). Flow cytometry documented an increased mean fluorescent intensity in alveolar macrophages after MI in mice injected with ^{VT680}Macrin (Fig. 5D–F). Also, the number of alveolar macrophages that had incorporated ^{VT680}Macrin expanded in mice after MI (Fig. 5G). Notably, ^{VT680}Macrin was not detectable in CD11c^{high}, MHCII^{high} and SiglecF^{low} lung leukocytes or Ly6G^{high} neutrophils (Online Fig. VG).

^{64}Cu-Macrin PET detects pulmonary inflammation in pigs and mice with pneumonia

When studying PET images obtained in ^{64}Cu-Macrin-injected pigs, we serendipitously observed lung areas with increased PET signal (Fig. 2F). This unexpected observation was also made in pigs without myocardial infarction (Fig. 6A). ^{64}Cu-Macrin distribution in pig lungs was heterogeneous, with higher uptake in inferior lung lobes. SUVmax obtained by PET differed significantly among lung regions, with high versus low uptake in individual animals (Fig. 6B), a finding that was replicated by ex vivo scintillation counting (Fig. 6C). Histological evaluation revealed increased macrophage content in alveoli and the interstitial space in certain lung regions (Fig. 6D–E), consistent with mild to moderate lung inflammation. A veterinarian pathologist noted the presence of low-grade chronic pneumonia, consistent with *Mycoplasma hyopneumoniae*[22]. Two lung CTs obtained in pigs with increased PET signal were interpreted as normal by a clinical radiologist, ruling out severe lung disease.

To follow up on these findings in pigs, we pursued ^{64}Cu-Macrin PET lung imaging using an experimental design that involved healthy control animals and mice infected with *Streptococcus pneumoniae*[23]. The bacterial burden in the lung (Fig. 7A–B) increased from day 3 to 4 after infection. Histological analysis revealed that mice with pneumonia had more lung macrophages (Fig. 7C–D). Gram-positive *S. pneumoniae* were identified in infected

mouse lungs only (Fig. 7E). Based on these data, we chose days 3 and 4 after infection for PET imaging of the lung. Sagittal and coronal PET/CT views of lungs obtained in control mice and mice with pneumonia illustrate increased CT lung density and robust ^{64}Cu-Macrin uptake (Fig. 7F). In vivo PET, ex vivo scintillation counting and autoradiography exposure revealed higher ^{64}Cu-Macrin uptake in the lungs of mice with pneumonia (Fig. 7G–I). Interestingly, ^{64}Cu-Macrin accumulation had already increased ~2-fold on day 3 after bacterial inoculation compared to the healthy lung (Fig. 7G–H), a time when the bioluminescence was still rising (Fig. 7B).

^{64}Cu-Macrin identifies atherosclerotic plaque inflammation in rabbits

Macrophages are key protagonists propelling inflammation in the arterial wall[3]. Driven by expanding macrophage numbers and their inflammatory actions, atherosclerotic plaques may rupture or erode, leading to organ ischemia, especially MI and stroke. Given that recent clinical data[24] demonstrated the therapeutic benefits of inhibiting inflammation in patients with cardiovascular disease, there is considerable interest in imaging assays for plaque macrophages. We therefore explored ^{64}Cu-Macrin PET/MRI in rabbits with atherosclerosis induced by Western diet and balloon injury. Using a clinical PET/MRI scanner, we observed 1.4-fold increased ^{64}Cu-Macrin uptake in the injured segments of the rabbits' abdominal aorta (Fig. 8A–B). Ex vivo scintillation counting (Fig. 8C) and autoradiography (Fig. 8D) confirmed higher activity in the aorta of rabbits with atherosclerosis. Immunohistochemical staining verified the presence of macrophages in rabbits' atherosclerotic lesions (Fig. 8E–F).

Finally, we explored cellular Macrin uptake in mice with atherosclerosis (Online Fig. VIIIA) by quantitative flow cytometry, relying on the well-established surface markers for key plaque cell populations in the mouse. Among aortic cells, Macrin was exclusively found in macrophages but not in CD45^{-} cells, fibroblasts, endothelial cells, monocytes and lymphocytes. Immunohistological examination of the mouse aortic root confirmed these FACS data (Online Fig. VIIIB).

Toxicity and dosimetry estimation

The documented sensitivity and specificity of the assay indicate its potential clinical usefulness. For first-in-human imaging, toxicity and dosimetry are warranted, which we report here. Standard toxicity evaluation showed no effect on body weight, food consumption, hematology blood counts, clinical chemistry or organ weights. No mortality or adverse clinical signs were observed up to 14 days after injection, when rats were sacrificed for autopsy and histopathology studies. The gross pathology and histopathology reports were normal, with no signs of toxicity.

Organ mass-adjusted extrapolation of the mouse biodistribution data (Online Table II) using the OLINDA/EXM dosimetry program yielded the human dose estimates shown in Table 1. The liver emerged as the dose-limiting organ with an effective dose of 0.143 ± 0.012 mSv/MBq. The organ with the second-highest uptake was the urinary bladder wall, followed by the kidneys. ^{64}Cu-Macrin uptake also occurred in the spleen. The average effective dose for ^{64}Cu-Macrin was 0.04 ± 0.001 mSv/MBq, which is higher than commonly used ^{18}F-FDG[25], but comparable to other copper-based PET tracers previously investigated in humans,

including ^{64}Cu-ATSM (0.036 mSv/MBq)[26] and ^{64}Cu-Trastuzumab (0.036 mSv/MBq)[27], and considerably lower than an I-124 labeled nanoparticle, ^{124}I-cRGDY-PEG-C-dot (0.162 mSv/MBq), currently undergoing a phase 1 trial for melanoma and malignant brain tumor PET imaging[28].

Discussion

Despite advances in clinical care, cardiovascular disease is still the global leading cause of death. While some conditions such as hyperlipidemia can be treated effectively, the immune system's role in atherosclerosis and heart failure is currently not harnessed therapeutically. This unused opportunity exists despite an urgent clinical need for therapeutics that act orthogonally to the current standard of care. The past decade provided new insight into the life cycle and functions of innate immune cells[29, 30]. Among these cells, macrophages are the most numerous residents in healthy tissues and expand further in atherosclerotic plaques that are poised to cause organ ischemia. Unresolved inflammatory activity of cardiac macrophages following MI results in adverse cardiac remodeling, fibrosis, left ventricular dilation and heart failure[3]. An improved understanding of macrophages' roles in cardiovascular disease and cancer fuels the current interest in targeting these cells therapeutically[31, 32]. Quantitative measurements of macrophage population size and their spatiotemporal variation in human patients would catalyze development of macrophage-targeted therapeutics. However, to date there is no clinically viable, specific tool for imaging macrophages in patients.

We here describe the first use of ^{64}Cu-Macrin for PET imaging of macrophage dynamics spanning different amplitudes, physiological states and cardiopulmonary pathologies: in newborn, septic and ischemic myocardium, in the lung after acute MI, in atherosclerotic plaques, and in subclinical and clinical pneumonia. Our data suggest that ^{64}Cu-Macrin PET is capable to assay tissue macrophages non-invasively in all these settings. The nanotracer emerged from continuous efforts to develop macrophage imaging agents. A first-generation dextran-based nanoparticle, called monocrystalline iron oxide nanoparticle (MION), was employed to image patients with prostate cancer[33], detecting the nanoparticles' iron oxide core by MRI. Similar materials were used to sense macrophages in atherosclerotic plaques[34] and acute myocardial infarction[35, 36]. The transition to nanoparticles derivatized with radioisotopes harnessed PET's higher sensitivity and quantitative capabilities[37]. Further optimization in size, surface chemistry and composition led to ^{89}Zr-labeled dextran nanoparticles made from the same coating material but without an iron oxide core[38]. To lower radiation burden and accelerate injection/imaging sequences, ultra-small 5 nm dextran nanoparticles were labeled with fluorine-18[39]. However, rapid renal clearance of these particles somewhat reduced macrophage uptake and sensitivity. This observation led to the current nanoparticle with ~20 nm diameter and a blood half-life of 45 min in rabbits. Macrin's favorable pharmacokinetic profile and high target cell avidity allowed macrophage detection in mice, rabbits and pigs with various inflammatory conditions. A previous study established its utility to detect tumor-associated macrophages in mice[15].

In addition to the dextran nanoparticle family, there are a number of alternatives for macrophage imaging; however, only a few have been evaluated in large animals and humans

and none are in routine use (reviewed in[31, 40]). Noteworthy examples are small molecule-based imaging agents that bind the chemokine receptor CCR2[13, 41] or the macrophage colony-stimulating factor 1 receptor (CSF1R)[14]. In addition to the longer blood half life of ^{64}Cu-Macrin, which may augment signal to background ratio through longer systemic availability, the specific targeting profile for macrophage subsets may differ. For instance, we observed Macrin signal in cardiac resident macrophage subsets which express low levels of CCR2. While not explicitly examined here, we expect that Macrin enriches in resident macrophages of most healthy tissues. The uptake of nanoparticles in a tissue of interest may depend, in addition to the properties of the nanomaterial[40], on macrophage (subset) abundance, activity and phagocytic history. For instance, we observed that the per cell fluorescence, which indicates the amount of individual ^{VT680}Macrin uptake into a cell, was higher in neonatal heart and lower in infarct macrophages. Therefore, the choice of macrophage imaging agent may depend on the specific application and currently emerging functions of macrophage subsets.

In addition to common inflammation imaging contexts such as atherosclerosis and myocardial infarction, we here employed ^{64}Cu-Macrin PET to image previously less well characterized biology. In newborn mice, which may still have active developmental pathways that facilitate better regeneration and scar-free infarct healing, ^{64}Cu-Macrin heart uptake was higher than in older mice. Flow cytometry of newborn hearts not only verified more cardiac macrophages per mg of myocardium but also documented a higher mean fluorescence intensity per cell, i.e. more Macrin nanoparticle uptake per individual macrophage. This observation indicates that the phenotype of cardiac macrophages in newborn hearts may be distinct, agreeing with a prior report that described a different, less inflammatory cardiac macrophage subset composition in neonatal mouse hearts[20]. A combination of enhanced macrophage functionalities needed for tissue repair, including phagocytosis, and lower inflammatory activity may contribute to the regenerative phenotype in the neonatal heart. In adult mice after MI, we observed higher Macrin uptake in primed alveolar macrophages, which then step up defenses against post-MI pneumonia, leading to better removal of bacteria from the alveolar space[4].

There is a growing need for assays to support macrophage-targeted drug development. Currently, the gold standards for macrophage quantification are flow cytometry and confocal microscopy, with extremely limited clinical utility. The ^{64}Cu-Macrin PET imaging applications tested here span conditions with large and subtle macrophage fluctuations, attesting to the dynamic range and utility of the assay. The large animal data, toxicity studies and human dosimetry estimates suggest that this latest-generation nanoparticle reporter is ready for first-in-human studies.

Supplementary Material

Refer to Web version on PubMed Central for supplementary material.

ACKNOWLEDGMENTS

We acknowledge Hye-Yeong Kim, PhD, who unfortunately was not able to contribute to the preparation of the final manuscript, for nanoparticle production and labeling, nanoparticle analysis, imaging and in vitro data collection and

analysis, contributing to figures and drafting the manuscript. We acknowledge Kaley Joyce, PhD, for editing the manuscript. We acknowledge Servier Medical Art for figure components.

Sources of funding

This work was funded in part by federal funds from the National Institutes of Health HL131495, HL139598, HL125428, HL131478, HL144072, CA220234, CA008748; from the European Union's Horizon 2020 research and innovation programme 667837, by the Netherlands Organization for Scientific Research (NWO; ZonMW Vici grant no. 016.176.622), the Massachusetts General Hospital Research Scholar Program, the German Research Foundation HO5279/1-2 and RO5071/1-1, German Heart Foundation, the Jung Foundation for Science and Research and by the American Heart Association 19PRE34380423.

Abbreviations

CLP	cecal ligation and puncture
PET	positron emission tomography
MRI	magnetic resonance imaging
CT	X-ray computed tomography
TTC	triphenyltetrazolium chloride
GFP	green fluorescent protein
MFI	mean fluorescent intensity
SUV	standard uptake value

References

1. Lavin Y, Mortha A, Rahman A, Merad M. Regulation of macrophage development and function in peripheral tissues. Nat Rev Immunol. 2015;15:731–744. [PubMed: 26603899]
2. Nahrendorf M. Myeloid cell contributions to cardiovascular health and disease. Nat Med. 2018;24:711–720. [PubMed: 29867229]
3. Swirski FK, Nahrendorf M. Cardioimmunology: the immune system in cardiac homeostasis and disease. Nat Rev Immunol. 2018;18:733–744. [PubMed: 30228378]
4. Hoyer FF, Naxerova K, Schloss MJ, Hulsmans M, Nair AV, Dutta P, Calcagno DM, Herisson F, Anzai A, Sun Y, Wojtkiewicz G, et al. Tissue-Specific Macrophage Responses to Remote Injury Impact the Outcome of Subsequent Local Immune Challenge. Immunity. 2019;51:899–914.e7. [PubMed: 31732166]
5. Panizzi P, Swirski FK, Figueiredo JL, Waterman P, Sosnovik DE, Aikawa E, Libby P, Pittet M, Weissleder R, Nahrendorf M. Impaired infarct healing in atherosclerotic mice with Ly-6C(hi) monocytosis. J Am Coll Cardiol. 2010;55:1629–1638. [PubMed: 20378083]
6. Engstrom G, Melander O, Hedblad B. Leukocyte count and incidence of hospitalizations due to heart failure. Circ Heart Fail. 2009;2:217–222. [PubMed: 19808343]
7. Madjid M, Awan I, Willerson JT, Casscells SW. Leukocyte count and coronary heart disease: implications for risk assessment. J Am Coll Cardiol. 2004;44:1945–1956. [PubMed: 15542275]
8. Maekawa Y, Anzai T, Yoshikawa T, Asakura Y, Takahashi T, Ishikawa S, Mitamura H, Ogawa S. Prognostic significance of peripheral monocytosis after reperfused acute myocardial infarction:a possible role for left ventricular remodeling. J Am Coll Cardiol. 2002;39:241–246. [PubMed: 11788214]
9. Aurora AB, Porrello ER, Tan W, Mahmoud AI, Hill JA, Bassel-Duby R, Sadek HA, Olson EN. Macrophages are required for neonatal heart regeneration. J Clin Invest. 2014;124:1382–1392. [PubMed: 24569380]

10. Nahrendorf M, Sosnovik DE, French BA, Swirski FK, Bengel F, Sadeghi MM, Lindner JR, Wu JC, Kraitchman DL, Fayad ZA, et al. Multimodality cardiovascular molecular imaging, Part II. Circ Cardiovasc Imaging. 2009;2:56–70. [PubMed: 19808565]
11. Rischpler C, Dirschinger RJ, Nekolla SG, Kossmann H, Nicolosi S, Hanus F, van Marwick S, Kunze KP, Meinicke A, Gotze K, et al. Prospective Evaluation of 18F-Fluorodeoxyglucose Uptake in Postischemic Myocardium by Simultaneous Positron Emission Tomography/Magnetic Resonance Imaging as a Prognostic Marker of Functional Outcome. Circ Cardiovasc Imaging. 2016;9:e004316. [PubMed: 27056601]
12. Thackeray JT, Derlin T, Haghikia A, Napp LC, Wang Y, Ross TL, Schäfer A, Tillmanns J, Wester HJ, Wollert KC, et al. Molecular Imaging of the Chemokine Receptor CXCR4 After Acute Myocardial Infarction. JACC Cardiovasc Imaging. 2015;8:1417–1426. [PubMed: 26577262]
13. Heo GS, Bajpai G, Li W, Luehmann HP, Sultan DH, Dun H, Leuschner F, Brody SL, Gropler RJ, Kreisel D, et al. Targeted PET Imaging of Chemokine Receptor 2+ Monocytes and Macrophages in the Injured Heart. J Nucl Med. 2020;16:3016–3023.
14. Horti AG, Naik R, Foss CA, Minn I, Misheneva V, Du Y, Wang Y, Mathews WB, Wu Y, Hall A, et al. PET imaging of microglia by targeting macrophage colony-stimulating factor 1 receptor (CSF1R). Proc Natl Acad Sci U S A. 2019;116:1686–1691. [PubMed: 30635412]
15. Kim H-Y, Li R, Ng TSC, Courties G, Rodell CB, Prytyskach M, Kohler RH, Pittet MJ, Nahrendorf M, Weissleder R. Quantitative Imaging of Tumor-Associated Macrophages and Their Response to Therapy Using 64Cu-Labeled Macrin. ACS Nano. 2018;12:12015–12029. [PubMed: 30508377]
16. Lee WW, Marinelli B, van der Laan AM, Sena BF, Gorbatov R, Leuschner F, Dutta P, Iwamoto Y, Ueno T, Begieneman MP, et al. PET/MRI of inflammation in myocardial infarction. J Am Coll Cardiol. 2012;59:153–163. [PubMed: 22222080]
17. Szychta W, Werys K, Barczuk-Falecka M, Postula M, Malek LA. Validation of performance of free of charge plugin for the open-source platform to perform cardiac segmentation in magnetic resonance imaging. Heart Beat Journal. 2018;3:83–89.
18. Jung S, Aliberti J, Graemmel P, Sunshine MJ, Kreutzberg GW, Sher A, Littman DR. Analysis of fractalkine receptor CX(3)CR1 function by targeted deletion and green fluorescent protein reporter gene insertion. Mol Cell Biol. 2000;20:4106–4114. [PubMed: 10805752]
19. Cerqueira MD, Weissman NJ, Dilsizian V, Jacobs AK, Kaul S, Laskey WK, Pennell DJ, Rumberger JA, Ryan T, Verani MS. Standardized myocardial segmentation and nomenclature for tomographic imaging of the heart. A statement for healthcare professionals from the Cardiac Imaging Committee of the Council on Clinical Cardiology of the American Heart Association. Int J Cardiovasc Imaging. 2002;18:539–542. [PubMed: 12135124]
20. Lavine KJ, Epelman S, Uchida K, Weber KJ, Nichols CG, Schilling JD, Ornitz DM, Randolph GJ, Mann DL. Distinct macrophage lineages contribute to disparate patterns of cardiac recovery and remodeling in the neonatal and adult heart. Proc Natl Acad Sci USA. 2014;111:16029–16034. [PubMed: 25349429]
21. Vagnozzi RJ, Maillet M, Sargent MA, Khalil H, Johansen AKZ, Schwanekamp JA, York AJ, Huang V, Nahrendorf M, Sadayappan S, et al. An acute immune response underlies the benefit of cardiac stem cell therapy. Nature. 2020;577:405–409. [PubMed: 31775156]
22. Maes D, Sibila M, Kuhnert P, Segales J, Haesebrouck F, Pieters M. Update on Mycoplasma hyopneumoniae infections in pigs: Knowledge gaps for improved disease control. Transbound Emerg Dis. 2018;65 Suppl 1:110–124. [PubMed: 28834294]
23. Davis RW, Eggleston H, Johnson F, Nahrendorf M, Bock PE, Peterson T, Panizzi P. In Vivo Tracking of Streptococcal Infections of Subcutaneous Origin in a Murine Model. Mol Imaging Biol. 2015;17:793–801. [PubMed: 25921659]
24. Ridker PM, Everett BM, Thuren T, MacFadyen JG, Chang WH, Ballantyne C, Fonseca F, Nicolau J, Koenig W, Anker SD, et al. Antiinflammatory Therapy with Canakinumab for Atherosclerotic Disease. N Engl J Med. 2017;377:1119–1131. [PubMed: 28845751]
25. Hays MT, Watson EE, Thomas SR, Stabin M. MIRD dose estimate report no. 19: radiation absorbed dose estimates from (18)F-FDG. J Nucl Med. 2002;43:210–214. [PubMed: 11850487]
26. Laforest R, Dehdashti F, Lewis JS, Schwarz SW. Dosimetry of 60/61/62/64Cu-ATSM: a hypoxia imaging agent for PET. Eur J Nucl Med Mol Imaging. 2005;32:764–770. [PubMed: 15785955]

27. Tamura K, Kurihara H, Yonemori K, Tsuda H, Suzuki J, Kono Y, Honda N, Kodaira M, Yamamoto H, Yunokawa M, et al. 64Cu-DOTA-trastuzumab PET imaging in patients with HER2-positive breast cancer. J Nucl Med. 2013;54:1869–1875. [PubMed: 24029656]
28. Benezra M, Penate-Medina O, Zanzonico PB, Schaer D, Ow H, Burns A, DeStanchina E, Longo V, Herz E, Iyer S, et al. Multimodal silica nanoparticles are effective cancer-targeted probes in a model of human melanoma. J Clin Invest. 2011;121:2768–2780. [PubMed: 21670497]
29. Lavin Y, Mortha A, Rahman A, Merad M. Regulation of macrophage development and function in peripheral tissues. Nature Reviews Immunology. 2015;15:731.
30. Ruparelia N, Chai JT, Fisher EA, Choudhury RP. Inflammatory processes in cardiovascular disease: a route to targeted therapies. Nat Rev Cardiol. 2017;14:133–144. [PubMed: 27905474]
31. Mulder WJ, Jaffer FA, Fayad ZA, Nahrendorf M. Imaging and nanomedicine in inflammatory atherosclerosis. Sci Transl Med. 2014;6:239sr1. [PubMed: 24898749]
32. Cassetta L, Pollard JW. Targeting macrophages: therapeutic approaches in cancer. Nat Rev Drug Discov. 2018;17:887–904. [PubMed: 30361552]
33. Harisinghani MG, Barentsz J, Hahn PF, Deserno WM, Tabatabaei S, van de Kaa CH, de la Rosette J, Weissleder R. Noninvasive detection of clinically occult lymph-node metastases in prostate cancer. N Engl J Med. 2003;348:2491–2499. [PubMed: 12815134]
34. Kooi ME, Cappendijk VC, Cleutjens KB, Kessels AG, Kitslaar PJ, Borgers M, Frederik PM, Daemen MJ, van Engelshoven JM. Accumulation of ultrasmall superparamagnetic particles of iron oxide in human atherosclerotic plaques can be detected by in vivo magnetic resonance imaging. Circulation. 2003;107:2453–2458. [PubMed: 12719280]
35. Sosnovik DE, Nahrendorf M, Deliolanis N, Novikov M, Aikawa E, Josephson L, Rosenzweig A, Weissleder R, Ntziachristos V. Fluorescence tomography and magnetic resonance imaging of myocardial macrophage infiltration in infarcted myocardium in vivo. Circulation. 2007;115:1384–1391. [PubMed: 17339546]
36. Alam SR, Shah AS, Richards J, Lang NN, Barnes G, Joshi N, MacGillivray T, McKillop G, Mirsadraee S, Payne J, et al. Ultrasmall superparamagnetic particles of iron oxide in patients with acute myocardial infarction: early clinical experience. Circ Cardiovasc Imaging. 2012;5:559–565. [PubMed: 22875883]
37. Nahrendorf M, Zhang H, Hembrador S, Panizzi P, Sosnovik DE, Aikawa E, Libby P, Swirski FK, Weissleder R. Nanoparticle PET-CT imaging of macrophages in inflammatory atherosclerosis. Circulation. 2008;117:379–387. [PubMed: 18158358]
38. Majmudar MD, Yoo J, Keliher EJ, Truelove JJ, Iwamoto Y, Sena B, Dutta P, Borodovsky A, Fitzgerald K, Di Carli MF, et al. Polymeric nanoparticle PET/MR imaging allows macrophage detection in atherosclerotic plaques. Circ Res. 2013;112:755–761. [PubMed: 23300273]
39. Keliher EJ, Ye Y-X, Wojtkiewicz GR, Aguirre AD, Tricot B, Senders ML, Groenen H, Fay F, Perez-Medina C, Calcagno C, et al. Polyglucose nanoparticles with renal elimination and macrophage avidity facilitate PET imaging in ischaemic heart disease. Nat Commun. 2017;8:14064. [PubMed: 28091604]
40. Weissleder R, Nahrendorf M, Pittet MJ. Imaging macrophages with nanoparticles. Nat Mater. 2014;13:125–138. [PubMed: 24452356]
41. Heo GS, Kopecky B, Sultan D, Ou M, Feng G, Bajpai G, Zhang X, Luehmann H, Detering L, Su Y, et al. Molecular Imaging Visualizes Recruitment of Inflammatory Monocytes and Macrophages to the Injured Heart. Circ Res. 2019;124:881–890. [PubMed: 30661445]

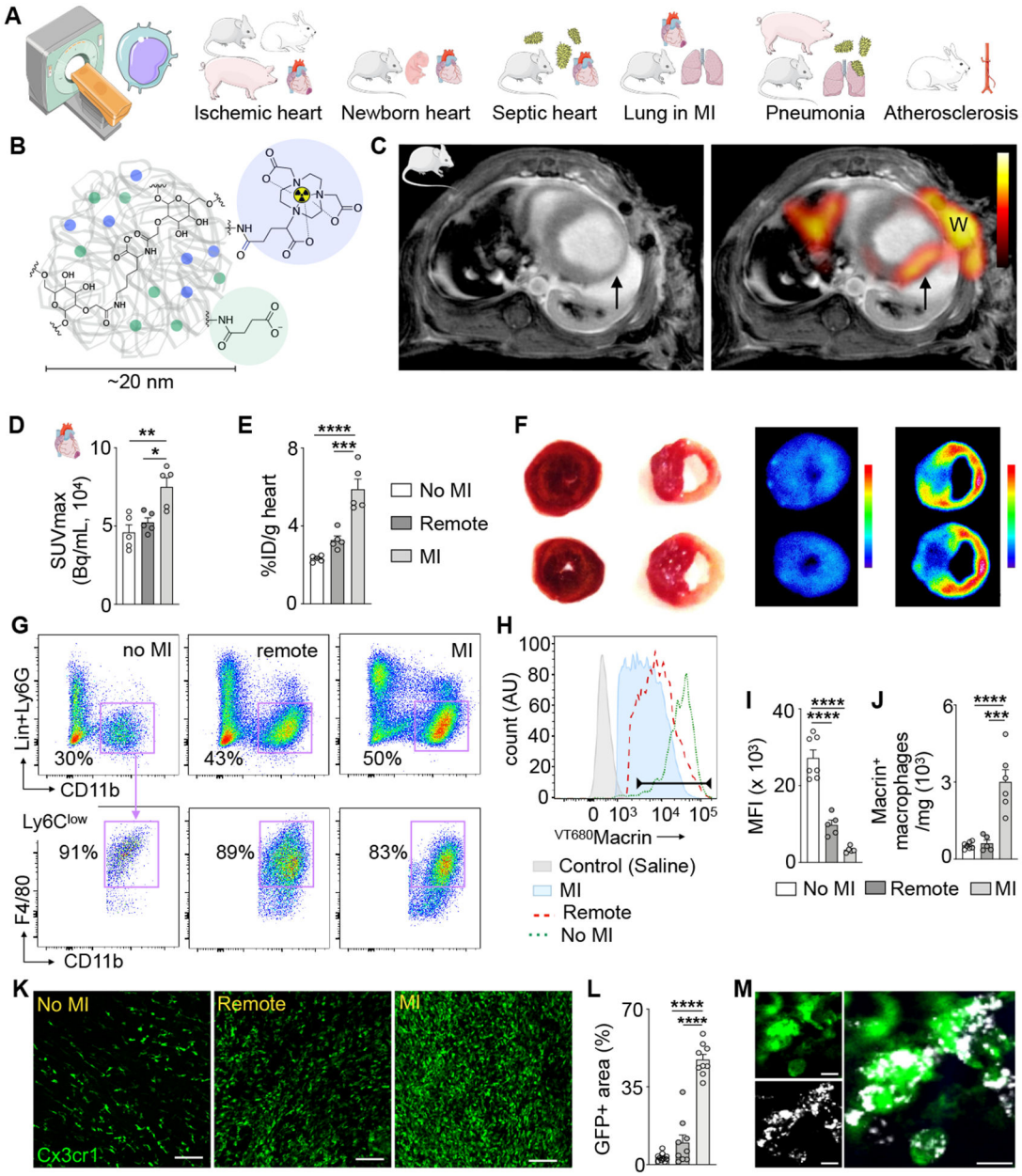

Figure 1. ^{64}Cu-Macrin PET imaging detects cardiac macrophage expansion following acute myocardial infarction in mice.

(A) Outline of macrophage imaging basket trial. **(B)** Schematic view of ^{64}Cu-Macrin polyglucose nanoparticle. **(C)** Short axis PET fused to MRI of mouse heart on day 5 after myocardial infarction (MI, arrow; W, surgical wound). Left image shows delayed enhancement MRI only, right is fused with PET. **(D)** In vivo PET signal, calculated as SUVmax in naive controls (no MI) and in the infarct (MI) and non-infarcted myocardium of mice with MI (remote). **(E)** Macrin accumulation in heart tissue by ex vivo scintillation counting and expressed as a percent injected dose per gram tissue (%ID/g). **(F)** TTC staining (left) and autoradiography (right) of mouse short axis rings from naive control and mouse with MI (right, infarct tissue is pale). **(G)** Flow plots of cardiac macrophages from control

mice and from remote and infarcted myocardium from mice with MI. Hearts were excised 24 h after IV injection of ^{VT680}Macrin. **(H)** Histogram of ^{VT680}Macrin uptake by cardiac macrophages in saline-injected naive controls (shaded grey), control (no MI, dotted green line), ischemic myocardium (MI, red dashed line) and remote myocardium in mice with MI (shaded blue). **(I)** ^{VT680}Macrin mean fluorescent intensity in cardiac macrophages and **(J)** ^{VT680}Macrin^{+} macrophage numbers. **(K)** Confocal microscopy of GFP expressing macrophages in Cx3cr1$^{GFP/+}$ mice on day 5 after MI (scale bar, 100 μm). **(L)** Quantitation of GFP^{+} area in groups as depicted in (**D**). **(M)** High-magnification confocal image of ^{VT680}Macrin (grey) and green macrophages (scale bar, 10 μm). Data are mean ± SEM. *P<0.05, **P<0.01, ***P<0.001, ****P<0.0001.

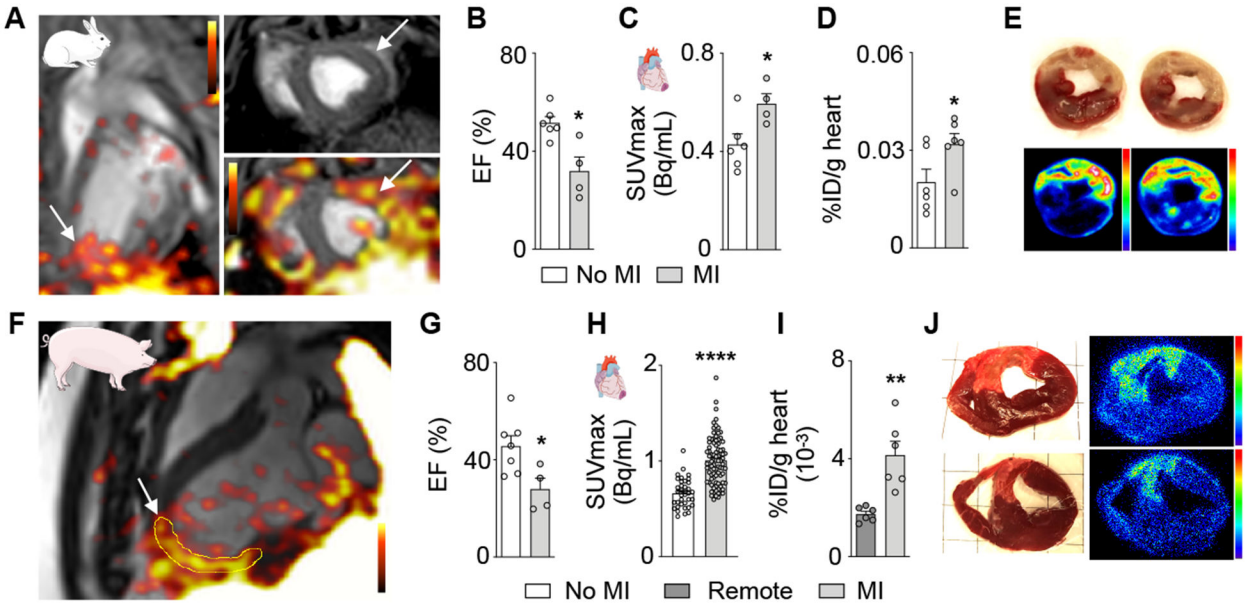

Figure 2. ^{64}Cu-Macrin PET imaging detects cardiac macrophage expansion following acute myocardial infarction in rabbits and pigs.

(A) PET/MR image of rabbit heart on day 3 after MI (arrows) and 24 h post injection of ^{64}Cu-Macrin. **(B)** Left ventricular ejection fraction (EF), assessed by MRI (n=4–6 rabbits per cohort). **(C)** In vivo ^{64}Cu-Macrin PET signal in rabbit hearts. **(D)** Ex vivo ^{64}Cu-Macrin uptake in rabbit heart (%ID/g). **(E)** TTC-stained rabbit heart tissue (upper row) shows pale infarcts with high activity on autoradiography exposure (bottom). **(F)** Long axis PET/MR image of a pig 3 days after MI (arrow), 24 h post administration of ^{64}Cu-Macrin. **(G)** EF in pigs assessed by MRI before and after MI (n=4–7 per cohort). **(H)** PET signal in infarcted and non-infarcted control myocardium. Each dot represents a myocardial segment of the AHA circumferential polar plot (n=4–7 pigs per cohort). **(I)** Ex vivo ^{64}Cu-Macrin uptake in pig hearts by scintillation counting (%ID/g). **(J)** TTC images (left) and autoradiography exposure (right) of infarcted pig heart. Data are mean ± SEM. *P<0.05, **P<0.01, ***P<0.001, ****P<0.0001.

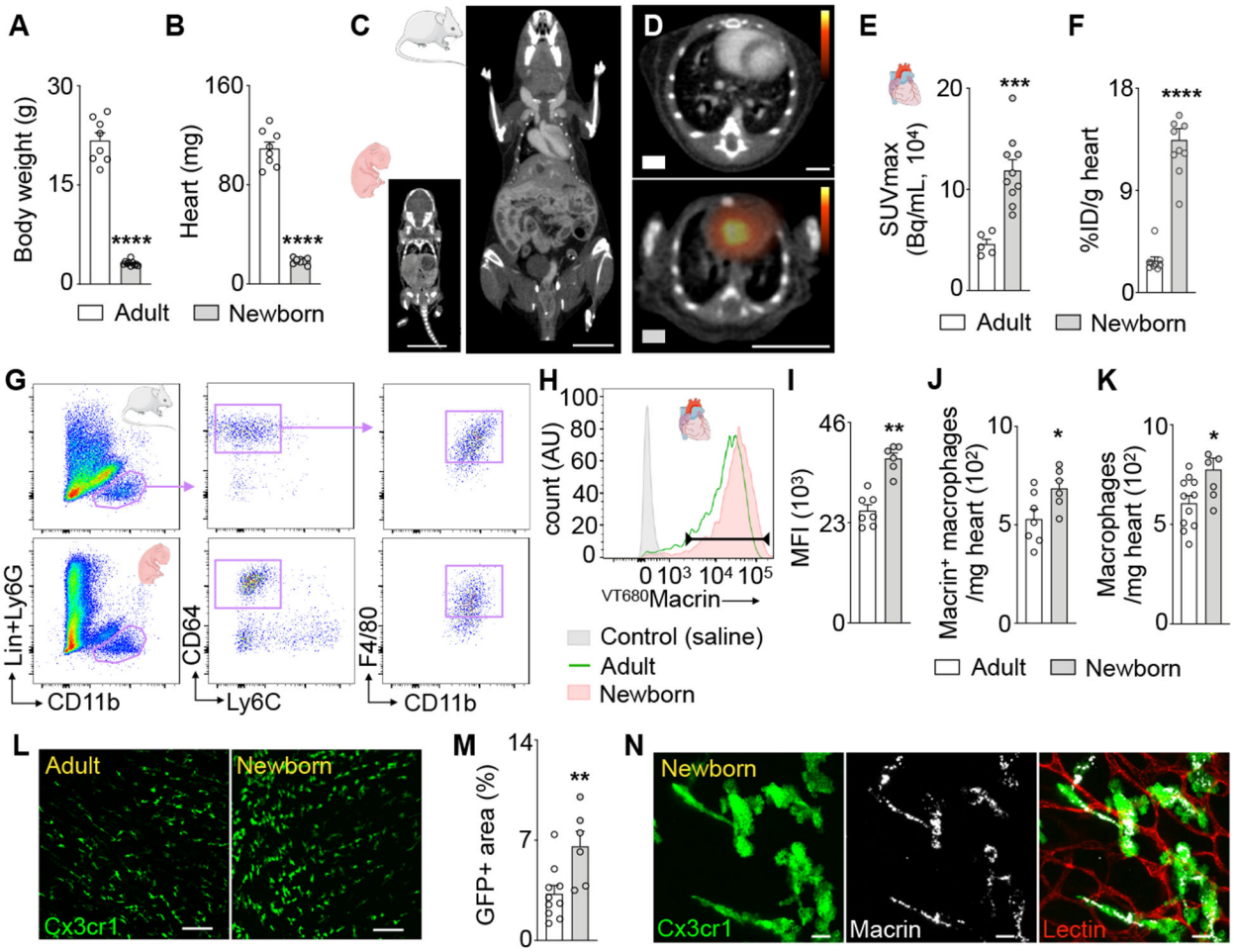

Figure 3. In vivo assessment of cardiac macrophages in newborn mice using ^{64}Cu-Macrin PET.

(A) Body and **(B)** heart weight of adult (9–10 weeks) and 5-day-old mice. **(C)** CT images of newborn and adult mouse (scale bar, 1cm). **(D)** PET/CT images visualize ^{64}Cu-Macrin uptake in adult (top) and newborn mouse heart (scale bar, 1cm). **(E)** ^{64}Cu-Macrin PET quantified as SUVmax and **(F)** ex vivo scintillation counting. **(G)** Flow cytometry gating for cardiac macrophages in adult and newborn mice. **(H)** Histogram showing ^{VT680}Macrin uptake in cardiac macrophages. Controls injected with saline (shaded grey), adult (solid green) and newborn mice (shaded orange). **(I)** Mean fluorescence intensity (MFI) in heart macrophages. **(J)** Number of ^{VT680}Macri^{n+} macrophages in the heart. **(K)** Macrophage numbers assessed by flow cytometry. **(L)** Confocal images of myocardium in Cx3cr1$^{GFP/+}$ mice (scale bar, 100 μm). **(M)** GFP^{+} area in hearts of Cx3cr1$^{GFP/+}$ mice by confocal microscopy. **(N)** ^{VT680}Macrin (grey) co-localizes with GFP^{+} macrophages in the heart of a newborn Cx3cr1$^{GFP/+}$ mouse (scale bar, 10μm). Data are mean ± SEM. **P*<0.05, ***P*<0.01, ****P*<0.001, *****P*<0.0001.

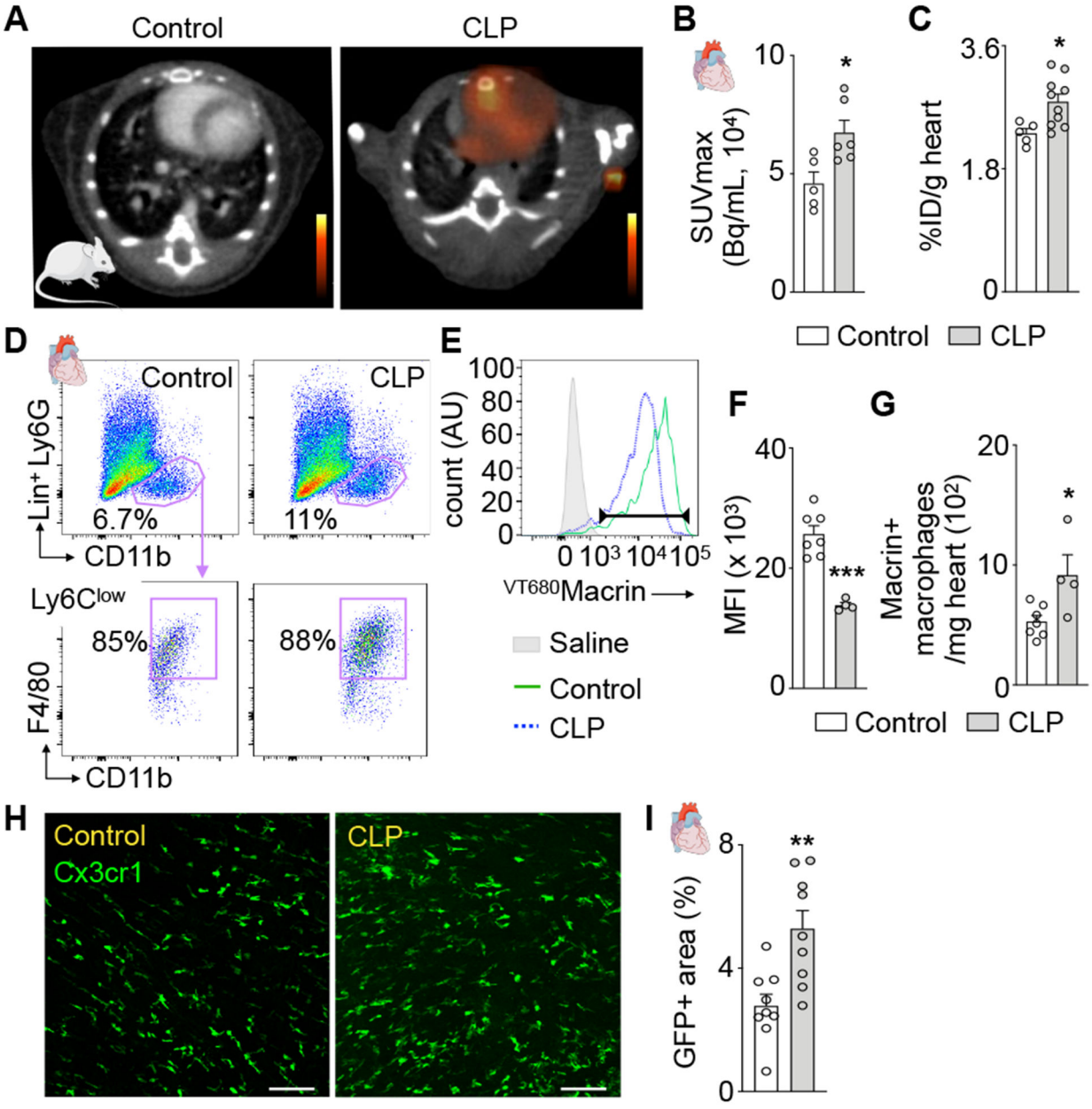

Figure 4. ^{64}Cu-Macrin PET detects cardiac macrophage dynamics in sepsis.

(A) PET/CT of the heart in a control mouse and a mouse after cecal ligation and puncture (CLP). **(B)** ^{64}Cu-Macrin uptake in myocardium by in vivo PET and **(C)** ex vivo scintillation counting. **(D)** Flow cytometry of cardiac macrophages in controls and mice after CLP. **(E)** Histogram of ^{VT680}Macrin uptake in cardiac macrophages. Saline-injected control group without CLP (shaded grey), control mice injected with ^{VT680}Macrin (solid green) and after CLP (dotted blue). **(F)** ^{VT680}Macrin mean fluorescent intensity (MFI) in cardiac macrophages. **(G)** Number of ^{VT680}Macrin^{+} cardiac macrophages. **(H)** Confocal microscopy of control and after CLP in Cx3cr1$^{GFP/+}$ mice (scale bar, 100 μm). **(I)** GFP-positive area in confocal heart images. Data are mean ± SEM. *P<0.05, **P<0.01, ***P<0.001.

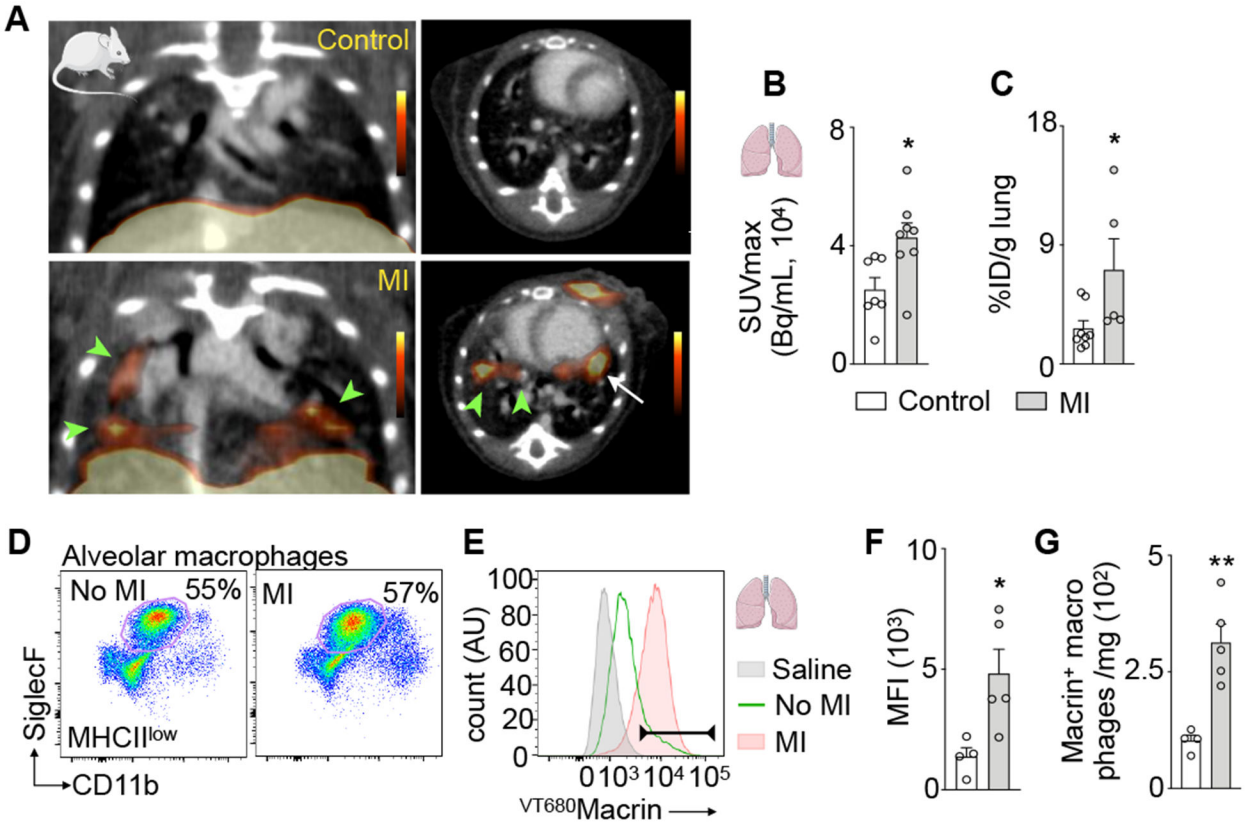

Figure 5. ^{64}Cu-Macrin PET detects lung macrophage dynamics after MI.

(A) Coronal and axial PET/CT images from control mouse (top) and mouse on day 5 after MI (bottom). Areas with high uptake in lung are indicated with arrowheads. Arrow indicates MI. **(B)** ^{64}Cu-Macrin signal in lung quantified by PET and **(C)** ex vivo scintillation counting. **(D)** Flow plots of alveolar macrophages in controls and mice after MI. **(E)** ^{VT680}Macrin fluorescence of alveolar macrophages; saline-injected controls (shaded grey), ^{VT680}Macrin injected control mice (solid green) and MI (shaded orange). **(F)** ^{VT680}Macrin mean fluorescence intensity (MFI) in alveolar macrophages. **(G)** Number of Macrin^{+} alveolar macrophages. Data are mean ± SEM. *P<0.05, **P<0.01, ***P<0.001.

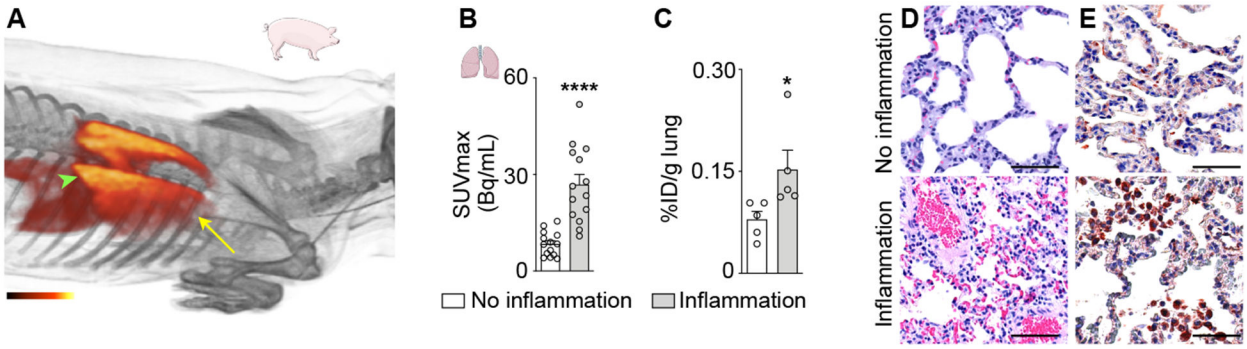

Figure 6. ^{64}Cu-Macrin PET imaging detects lung inflammation in pigs.

(A) 3-dimensional PET/MRI reconstruction of pig thorax 24 h post injection of ^{64}Cu-Macrin. Arrowhead indicates basal lung region with high PET signal; arrow indicates apical lung region with lower ^{64}Cu-Macrin uptake. **(B)** ^{64}Cu-Macrin accumulation in lungs of n=8 pigs as analyzed by in vivo PET (SUVmax in multiple lung region of interests) and **(C)** ex vivo scintillation counting of lung tissues. **(D)** H&E histology and **(E)** immunohistochemistry for macrophages from normal (top) and inflamed (bottom) pig lung regions (scale bar, 50 μm).

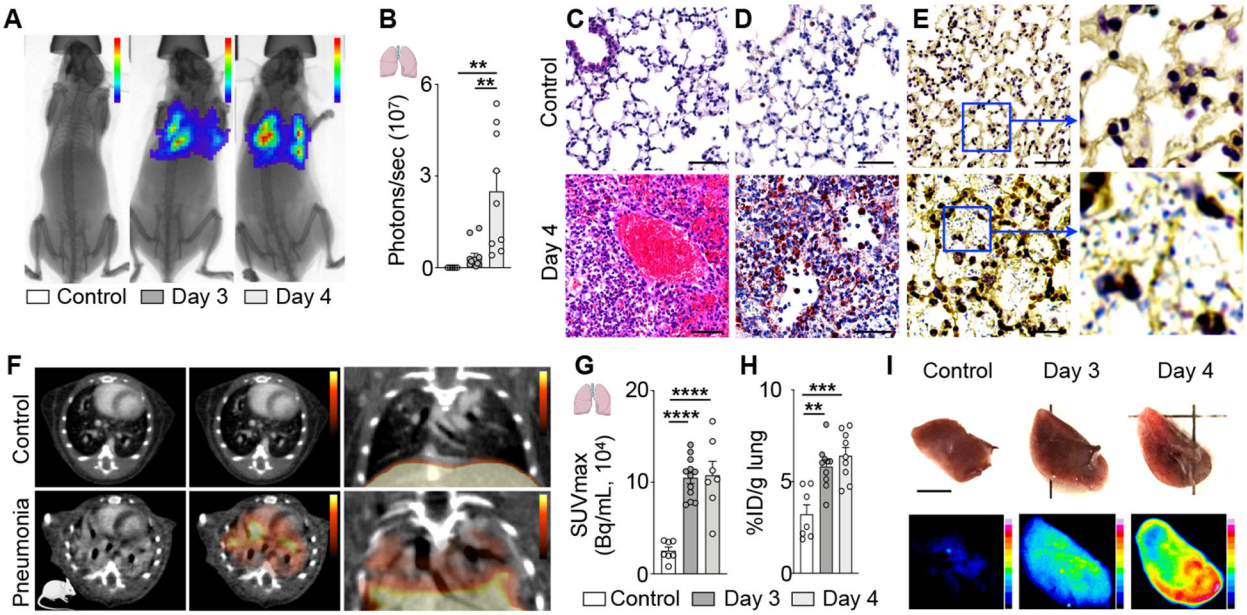

Figure 7. ^{64}Cu-Macrin PET imaging detects lung inflammation in mice.

(A) Bioluminescent / X-ray images of control mouse (left) and mice with pneumonia on days 3 and 4 after inoculation with bioluminescent Streptococcus pneumoniae. **(B)** Bacterial burden assessed by bioluminescence. **(C-E)** Lung histology from uninfected controls (top) and mice with pneumonia (bottom, day 4; scale bar, 50 μm), **(C)** H&E, **(D)** IHC for mouse macrophages (brown) and **(E)** gram-staining for streptococcus pneumoniae (pale blue). **(F)** PET/CT images from control mouse (top) and mouse with pneumonia (bottom, day 4 after infection). **(G)** ^{64}Cu-Macrin lung uptake by in vivo PET and **(H)** ex vivo scintillation counting. **(I)** Visualization of ^{64}Cu-Macrin accumulation in mouse lungs by autoradiography (scale bar, 5 mm). Data are mean ± SEM. **P*<0.05, ***P*<0.01, ****P*<0.001, *****P*<0.0001.

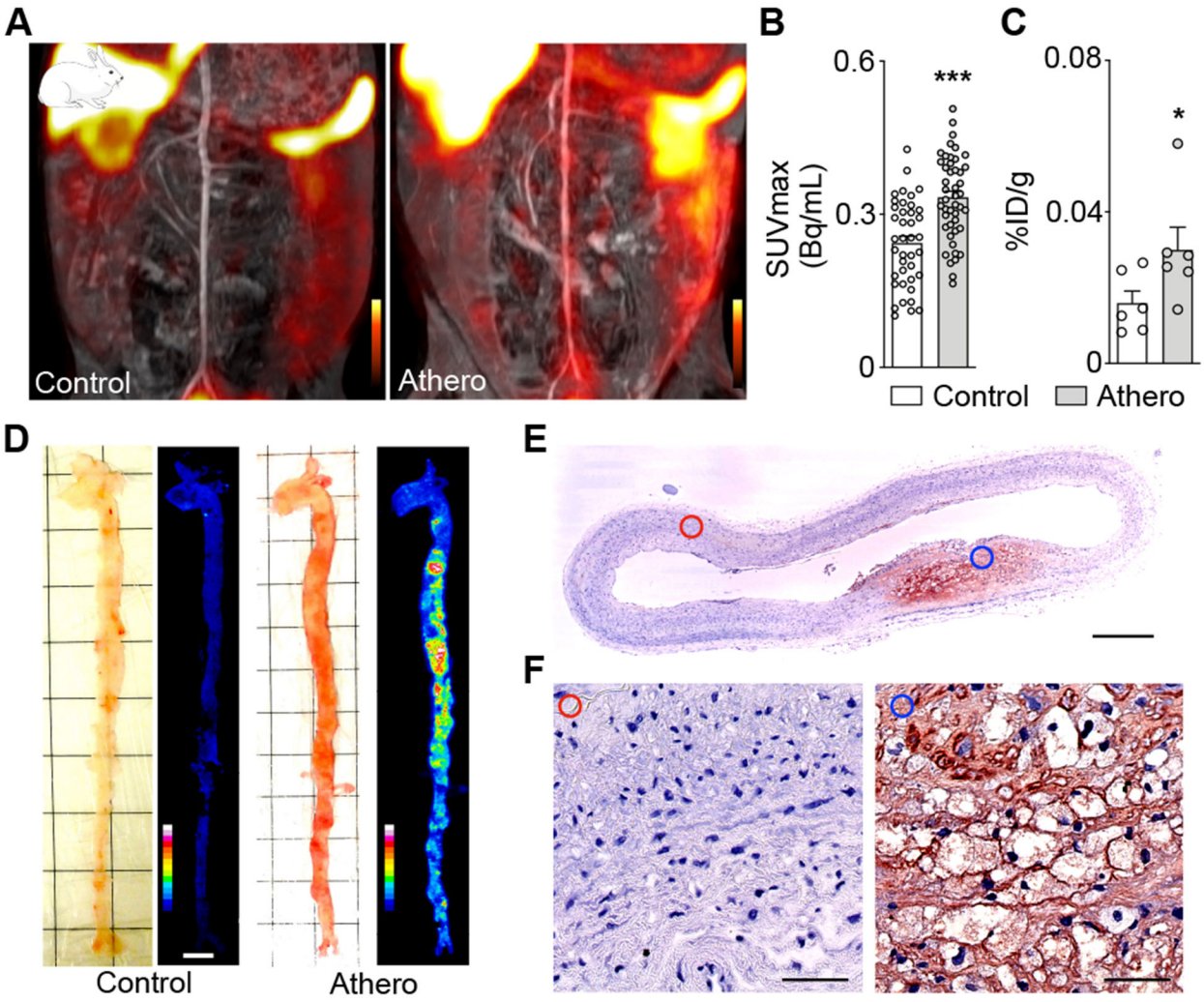

Figure 8. ^{64}Cu-Macrin PET imaging of atheromatous plaques in rabbits.

(A) Coronal PET/MR images of the abdominal aorta in a control rabbit (left) and a rabbit with atherosclerosis (right) 24 h post injection. **(B)** In vivo ^{64}Cu-Macrin PET signal in aortic segments (n=6 rabbits per group). **(C)** ^{64}Cu-Macrin uptake in aortae as measured by ex vivo scintillation counting. **(D)** Bright-field image (left) and autoradiography (right) of dissected rabbit aortae (scale bar, 1 cm). **(E)** Immunohistochemical staining for macrophages in rabbit aortae (scale bar, 0.5 mm). **(F)** Images from normal region (left, red circle) and atherosclerotic lesion (right, blue circle) (scale bar, 50 μm). Data are mean ± SEM. *P<0.05, ***P<0.001.

Table 1.

Human radiation dose estimates for ^{64}Cu-Macrin using Organ Level INternal Dose Assessment (OLINDA/EXM).

Estimated human organ dosimetry (mSv/MBq, mean ± SD) was extrapolated from the mouse biodistribution data (Table S1).

Organ	Adult male (mSv/MBq)	Adult female (mSv/MBq)	Adult (mSv/MBq)
Adrenals	0.018 ± 0.004	0.020 ± 0.004	0.019 ± 0.002
Brain	0.004 ± 0.001	0.004 ± 0.001	0.004 ± 0.001
Breast	0.010 ± 0.003	0.011 ± 0.003	0.011 ± 0.001
Gallbladder Wall	0.023 ± 0.004	0.024 ± 0.004	0.023 ± 0.001
LLI Wall	0.053 ± 0.016	0.058 ± 0.017	0.055 ± 0.004
Small Intestine	0.024 ± 0.002	0.026 ± 0.003	0.025 ± 0.002
Stomach Wall	0.019 ± 0.000	0.022 ± 0.000	0.021 ± 0.002
ULI Wall	0.046 ± 0.014	0.052 ± 0.015	0.049 ± 0.004
Heart Wall	0.013 ± 0.001	0.021 ± 0.002	0.017 ± 0.006
Kidneys	0.109 ± 0.095	0.109 ± 0.083	0.109 ± 0.000
Liver	0.135 ± 0.083	0.152 ± 0.098	0.143 ± 0.012
Lungs	0.017 ± 0.001	0.022 ± 0.001	0.019 ± 0.003
Muscle	0.007 ± 0.000	0.008 ± 0.000	0.008 ± 0.001
Ovaries	N/A	0.032 ± 0.019	0.032 ± 0.019
Pancreas	0.017 ± 0.000	0.019 ± 0.000	0.018 ± 0.001
Red Marrow	0.027 ± 0.004	0.029 ± 0.004	0.028 ± 0.002
Osteogenic Cells	0.029 ± 0.004	0.039 ± 0.004	0.034 ± 0.007
Skin	0.009 ± 0.003	0.010 ± 0.003	0.010 ± 0.001
Spleen	0.043 ± 0.009	0.048 ± 0.014	0.045 ± 0.004
Testes	0.053 ± 0.062	N/A	0.053 ± 0.062
Thymus	0.011 ± 0.003	0.012 ± 0.004	0.012 ± 0.001
Thyroid	0.010 ± 0.003	0.011 ± 0.004	0.010 ± 0.001
Urinary Bladder Wall	0.097 ± 0.003	0.151 ± 0.003	0.124 ± 0.038
Uterus	N/A	0.026 ± 0.007	0.026 ± 0.007
Total Body	0.017 ± 0.000	0.019 ± 0.000	0.018 ± 0.002
Effective dose	0.040 ± 0.018	0.041 ± 0.011	0.040 ± 0.001